Atmospheric Environment 165 (2017) 99–110

Contents lists available at ScienceDirect

Atmospheric Environment

journal homepage: www.elsevier.com/locate/atmosenv

Paracas dust storms: Sources, trajectories and associated meteorological conditions

F. Briceño-Zuluaga [a, b, c, d, *], A. Castagna [d], J.A. Rutllant [e, f], V. Flores-Aqueveque [g], S. Caquineau [b, c], A. Sifeddine [a, b, c], F. Velazco [h], D. Gutierrez [h, i], J. Cardich [a, b, c]

[a] Programa de Geoquímica, Universidade Federal Fluminense - UFF, Niterói, RJ, Brazil
[b] IRD-Sorbonne Universités (UPMC, CNRS-MNHN), LOCEAN, IRD France-Nord, Bondy, France
[c] LMI PALEOTRACES (IRD-France, UPMC-France, UA-Chile, UFF-Brazil, UPCH-Peru)
[d] Laboratório de Radioecologia e Mudanças Globais (LARAMG), Universidade do Estado do Rio de Janeiro – UERJ, Rio de Janeiro, RJ, Brazil
[e] Departamento de Geofísica, Fac. Ciencias Físicas y Matemáticas, Universidad de Chile, Chile
[f] Center for Advanced Studies in Arid Zones (CEAZA), La Serena, Chile
[g] ARQMAR, Centre for Maritime Archaeology Research of the South Eastern Pacific, Escuela de Ingeniería, Universidad Santo Tomás, Chile
[h] Instituto del Mar del Peru IMARPE, Esquina Gamarra y General Valle s/n, Callao 22000, Peru
[i] Programa de Maestría de Ciencias del Mar, Universidad Peruana Cayetano Heredia UPCH, Peru

HIGHLIGHTS

- Strong winds are forced by alongshore pressure gradients between Pisco and Arica.
- Paracas events are associated with the strengthening of anticyclonic conditions.
- HYSPLIT outputs were able to reproduce trajectories and dust dispersion plumes.
- The presence of the aeolian signal in the continental shelf sediments is assessed.
- Population towns can be health affected by high aeolian particle concentrations.

ARTICLE INFO

Article history:
Received 2 December 2016
Received in revised form
8 June 2017
Accepted 10 June 2017
Available online 12 June 2017

Keywords:
Aeolian transport
HYSPLIT trajectories
Dust storms
Southern Peru
Synoptic-scale meteorological patterns

ABSTRACT

Dust storms that develop along the Pisco-Ica desert in Southern Peru, locally known as “Paracas” winds have ecological, health and economic repercussions. Here we identify dust sources through MODIS (Moderate Resolution Imaging Spectroradiometer) imagery and analyze HYSPLIT (Hybrid Single Particles Lagrangian Integrated Trajectory) model trajectories and dispersion patterns, along with concomitant synoptic-scale meteorological conditions from National Centers for Environmental Prediction/National Center for Atmospheric Research reanalysis (NCEP/NCAR). Additionally, surface pressure data from the hourly METeorological Aerodrome Report (METAR) at Arica (18.5°S, 70.3°W) and Pisco (13.7°S, 76.2°W) were used to calculate Alongshore (sea-level) Pressure Gradient (APG) anomalies during Paracas dust storms, their duration and associated wind-speeds and wind directions. This study provides a review on the occurrence and strength of the Paracas dust storms as reported in the Pisco airfield for five-year period and their correspondence with MODIS true-color imagery in terms of dust-emission source areas. Our results show that most of the particle fluxes moving into the Ica-Pisco desert area during Paracas wind events originate over the coastal zone, where strong winds forced by steep APGs develop as the axis of a deep mid-troposphere trough sets in along north-central Chile. Direct relationships between Paracas wind intensity, number of active dust-emission sources and APGs are also documented, although the scarcity of simultaneous METAR/MODIS data for clearly observed MODIS dust plumes prevents any significant statistical inference. Synoptic-scale meteorological composites from NCEP/NCAR reanalysis data show that Paracas wind events (steep APGs) are mostly associated with the strengthening of anticyclonic conditions in northern Chile, that can be attributed to cold air advection associated with the incoming trough. Compared to the MODIS images, HYSPLIT outputs were able to spatially reproduce trajectories and dust dispersion plumes during the Paracas wind storms. HYSPLIT trajectories revealed

* Corresponding author. Laboratório de Radioecologia e Mudanças Globais (LARAMG), Universidade do Estado do Rio de Janeiro – UERJ, Rio de Janeiro, RJ, Brazil.
E-mail address: franciscojavier@id.uff.br (F. Briceño-Zuluaga).

http://dx.doi.org/10.1016/j.atmosenv.2017.06.019

that part of the wind-eroded lithological material can be transported downwind several kilometers along the Peruvian coast and also deposited over the nearby coastal ocean, giving support to the presence of an aeolian signal in continental shelf sediments, of great importance for paleoenvironmental studies.

1. Introduction

The South Peruvian and North Chilean coasts are characterized by their extreme aridity and intense alongshore equatorward winds. Along the Peruvian coast, the Pisco - San Juan region (~14–15°S) presents the most intense alongshore surface winds driving the principal coastal upwelling focus in Southern Peru (Gutiérrez et al., 2011; Suess et al., 1987; Sydeman et al., 2014). This feature, in combination with arid environmental and geomorphological conditions brings on episodic aeolic erosion events (dust storms). These strong winds, with typical speeds exceeding 10–15 m s^{-1}, are locally known as Paracas Winds (PW), blowing from the South – Southeast (S-SE) over the extremely dry coastal desert. On average, PW occur 4 to 5 times per year, mainly in the afternoons towards the end of austral winter (Escobar, 1993; Quijano, 2013). PW can heavily impact on economic activities and on the health of the local population, air quality and visibility conditions (Achudume and Oladipo, 2009; Shao et al., 2011; Soy et al., 2016).

Winds along the adjacent coastal ocean are often shaped as an alongshore atmospheric low-level jet (e.g. Dewitte et al., 2011; Rahn and Garreaud, 2013) leaving a cloud-free coastal strip extending 20–30 km offshore. This jet shares some characteristics with the coastal jet off 30°S over central Chile, as reported in Garreaud and Muñoz (2005) and Muñoz and Garreaud (2005). According to these authors, the presence of coastal mountain ranges oriented in the alongshore direction, force a semi-geostrophic wind equilibrium; their strength being directly proportional to the alongshore pressure gradient (APG) (e.g. Rahn and Garreaud, 2013). Based on Climate Forecast System Reanalysis (CFSR) data (Saha et al., 2010) at 00:00 UTC [19:00 Local Time (LT)], Rahn and Garreaud (2013) have reported a maximum climatological APG along the Peruvian coast off Pisco in austral winter (JJA), when the Southeast Pacific Subtropical High (SPSH) reaches its northernmost position. Although PW represents a phenomenon with local and regional significance, it has only been discussed in a limited number of reports (e.g. Takahashi et al., 2011; Quijano, 2013), particularly in terms of dust sources, trajectories and dust plume dispersion.

The Hybrid Single-Particle Lagrangian Integrated Trajectory model (HYSPLIT) for dust emissions (Stein et al., 2015; Draxler and Hess, 1998; Rolph, 2016), complemented by visual inspection of daily satellite imagery, presents itself as an alternative or complement to the fieldwork (Wang et al., 2011). HYSPLIT is a particle dispersion, trajectory and back-trajectory model based on Eulerian and Lagrangian dynamics. The model algorithm for the onset of dust emission uses the concept of a threshold surface friction velocity that must be exceeded at any given place and time (Draxler et al., 2001; Kok et al., 2012; Marticorena, 2014).

The main focus of this study is to provide a synoptic overview of the PW through assessing sources, emission patterns, trajectories, and downwind particle concentrations during their lifespan. The first section of this paper presents the local context of the study area and describes the methodology used. The second section details results from the HYSPLIT model simulations and assesses its performance. A characterization of the attending synoptic-scale meteorological conditions associated to these events is also included. The last section summarizes our main conclusions.

2. Data and methods

2.1. Geomorphological setting

The area chosen for the PW synoptic study spans from 76°48′W/15°26′S to 74°27′W/13°18′S [World Geodetic System 84 datum (WGS84)], from the Paracas peninsula to Northwest Arequipa (Fig. 1). According to Haney and Grolier (1991); Schweigger (1968) and Gay (2005) this area is characterized by the lack of vegetation, high aeolian deposits and strong winds. These climatic and geomorphologic features create favorable conditions for wind erosion resulting in dust storms.

2.2. Identification and delimitation of emission sources

Daily images from true color spectroradiometer MODIS of both Terra 10:30 LT (13:30 UTC) and Aqua 13:30 LT (18:30 UTC) satellites with moderate resolution (250 × 250 m by pixel) were analyzed for the years 2008, 2009, 2010, 2013, 2014 and 2015. Data were not available for the period 2011–2012 (LANCE server, which provides the pan-sharpened true color composites used in this study, had a hardware failure with irrecoverable data loss during the period of data gathering for this study. Data were scheduled for reprocessing, but available only after this study was concluded). These data were processed and freely distributed by the Land, Atmosphere Near real-time Capability for EOS (LANCE https://earthdata.nasa.gov/earth-observation-data/near-real-time/rapid-response/modis-subsets).

Among all the 2289 available images, blurry, cloudy overcast or incomplete ones were discarded, leading to a selection of 2269 sharp images with surface view, partly or unobstructed by clouds and therefore suitable for the identification of aeolian dust emissions and for the delimitation of their associated sources. This procedure was performed by visual inspection of true color composites, only considering sources where dust emission could be clearly discriminated. After that, geographical information system software (QGIS Development Team, 2016) was implemented in order to perform polygons (Stetch templates) of the source emission areas identified. Thus, MODIS (Aqua/Terra) images were manually worked one by one identifying dust sources as they were observed. Thus, a collage representing the sources as a whole was obtained. Finally, a total of 21 dust-source areas were identified (see results Fig. 3). After that, we reviewed back all the images with the aim of reconfirming these areas and see if they emitted more than once (Table 1S). Locations of the centers of all these areas were then introduced as a grid input in the HYSPLIT trajectories and the dust emission model. Polygons were selected regardless of how many times they constituted a dust source (i.e. a threshold in surface friction velocity for this area was exceeded).

2.3. Model description

To assess the general pattern of particle motion during PW

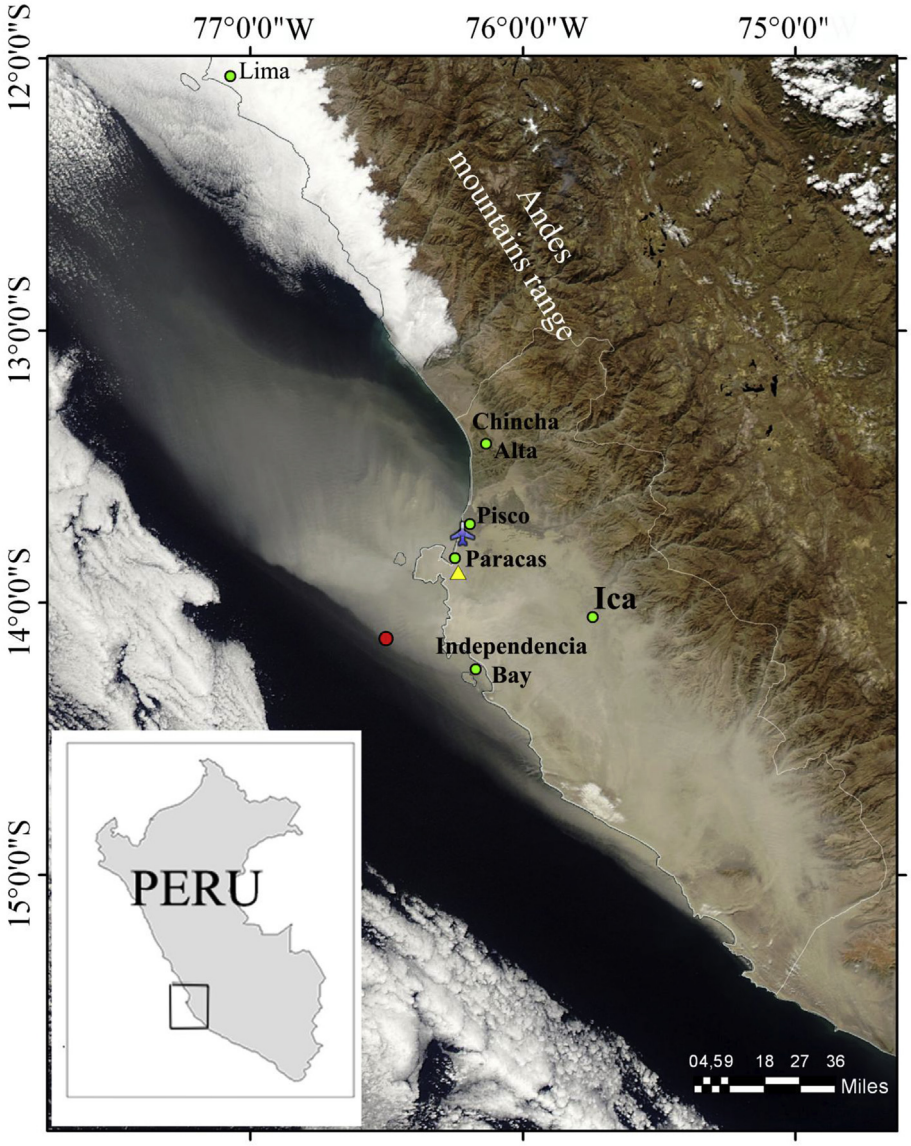

Fig. 1. Study area and illustration of a Paracas dust storm at Ica and Paracas regions through MODIS Aqua-Terra, true color image with surface reflectance (NASA) for 23-07-2014. The yellow triangle identifies the Big Spring Number Eight (BSNE) experimental station. The red dot is the location of the marine sediment core analyzed in Briceño Zuluaga et al. (2016). Pisco airfield is also identified. (For interpretation of the references to colour in this figure legend, the reader is referred to the web version of this article.)

events, trajectory frequency analyses were performed for all dust emission sources/areas, as identified with satellite imagery, using the GDAS 0.5° × 0.5° data, except for February 2010 when only the coarser GDAS 1° × 1° data were available. Taking into account the 21 identified centers of emission areas trajectories were traced with HYSPLIT for 48 h in 30-minute steps starting 3 h before and ending 3 h after each dust emission event (i.e., 13 possible trajectories per dust event), using the satellite overpass time as reference. This approach gives a general overview of the trajectories of dust-carrying air masses, as well as the frequency of their corresponding pathways, as approximated by air masses passing over the center of each emission source at ground level (10 m).

HYSPLIT also allows for the simulation of emission, dispersion and deposition of dust particles (Stein et al., 2015; Draxler and Hess, 1998; Draxler et al., 2001). For the onset of dust emission from a desert soil, the local wind velocity must exceed the threshold surface friction velocity of the considered soil which is controlled by its surface roughness. This parameter depends, among others, on soil particle-size distribution (Iversen and White, 1982; Kok et al., 2012; Marticorena and Bergametti, 1995; Marticorena, 2014; Shao, 2009). Since threshold surface friction velocities change widely in space and time, their representation in dust emission models for large-scale studies is complicated, especially in areas where detailed soil characteristics are not available.

As a consequence, a simpler version of the dust emission module has been used in this study, in which the emission flux (E) is calculated according to the relationship first proposed by Westphal et al. (1987) which is not dependent upon soil characteristics: $E = 0.01\ U^{*4}A$, where U^* (ms^{-1}) is the surface friction velocity and A (m^2) the area of the emission source. In this version, it is assumed that dust emissions only occur when the surface friction velocity exceeds a constant threshold value of $U^*t = 0.28\ ms^{-1}$ (Escudero et al., 2006). This value of 0.28 ms^{-1} corresponds to the surface threshold friction velocity assigned to "active sand sheet" soil type category (Draxler et al., 2001), largely present in central and southern Peru (Haney and Grolier, 1991).

In order to characterize the dispersion plume during a PW dust storm, the emission model was run for 30 h starting at 10:00 LT (15:00 UTC) during the July 23, 2014 dust event. This PW event was chosen as MODIS (Aqua and Terra) images show it as the largest and most massive dust emission within the study period. Since the emission model requires meteorological data to provide feedback as the dust plume develops, their spatial resolution and accuracy depends on the density of these data. In this study, 3-hour time resolution data from GDAS (0.25° × 0.25° spatial resolution) were used. Each cycle of the model runs with 50000 particles, with a maximum of 100000 particles per dust emission event. The dispersion of the dust plume results from a turbulent velocity component added to the mean particle motion. Ground-level concentrations are then calculated as the mean within the first 100 m above ground (Draxler and Hess, 1998; Rolph, 2016; Stein et al., 2015). HYSPLIT also allows for the control of other parameters like density, shape and particle diameter of the dust plume simulated. This allows for the assessment of grain size particles determining the dust transport range. Since both dust emission and transport are grain size-selective processes, assessing the particle grain sizes that most contribute to dust plumes is of utmost importance for dispersion modeling.

2.4. Lithological wind eroded grain size distributions and definition of HYSPLIT-modeled aeolian grain size patterns

In order to assess the aeolian grain size fractionation over the Paracas peninsula, 15 samples were collected by means of Big Spring Number Eight [BSNE; Fryrear (1986)] sand traps during a field experiment carried out in 2008 [Experimental Aeolian Station (EAS)] in the Paracas peninsula (−76° 25′W; −13° 86′S) (yellow triangle on Fig. 1). This experiment also allowed for the assessment of particle-uplift capability, erosion and grain-size distributions on Paracas soils. Three BSNE traps were fixed on the windward side of a vertical mast at 14 cm, 50 cm and 100 cm above the ground level. The material accumulated in each trap was carefully collected after five time intervals (from May to December), lasting approximately one month each. During that period, seven Paracas events, from moderate to strong (as in Escobar, 1993), were recorded. Grain size distribution of these collected samples was determined by dry sieving (Ingram, 1971). In addition, granulometric results were classified according to size class proposed by Wentworth (1922).

Additional size fractionation by gravitational settling occurs during short to long range transport. A decreasing trend in the coarser portion of the grain size distribution is therefore expected as the dust plume moves away from its source region. Studying the terrigenous fraction of Pisco continental shelf laminated sediments (Fig. 1), Briceño Zuluaga et al. (2016) found that the grain sizes in laminated sediments off the Paracas peninsula featured four granulometric modes: ~3 μm, ~10 μm, ~50 μm and 90 μm. While the last two coarser modes, also present in BSNE grain sizes have been uniquely linked to PW aeolian erosion by these authors finer particles (~3 μm and 10 μm) were associated to undefined and fluvial origin, respectively. Since we are mainly interested in relatively long and median aeolian range transport, we have chosen all four grain sizes modes found by Briceño-Zuluaga et al. (2016) as input data for HYSPLIT. A shape factor of 1.0 (spherical particles) and a density of 2.6 g cm^{-3} associated to quartz and feldspar (Albite), typically present in the composition of the Paracas soils (unpublished data) and continental shelf marine sediments (Sifeddine et al., 2008), were also used.

2.5. Meteorological data

For all PW events, anomalies in the forcing of coastal winds associated with alongshore pressure gradients (APG) were obtained from hourly METAR (METeorological Aerodrome Reports) surface pressure data (www.ogimet.com) at Arica (18.5°S; hereafter "SCAR") and Pisco (13.7°S; hereafter "SPSO") airfields. The analysis spans a 5-year (2007–2011) period in which only afternoon reports (17:00 to 22:00 UTC: 12:00 to 17:00 h LT) have been considered, given that most of the PW events are present as dust storms (DS) in the METAR code during this period. Due to differences in station altitude for calculating the APGs, station pressure values were reduced to sea-level according to the International Standard Atmosphere (http://www-mdp.eng.cam.ac.uk/web/library/enginfo/aerothermal_dvd_only/aero/atmos/atmos. html) by adding 1 hPa every 8 m altitude, yielding + 7 hPa at SCAR (50 m a.s.l) and +1.5 hPa at SPSO (13 m a.s.l). This is a reasonable reduction rate since atmospheric pressure is rounded to 1 hPa in METAR messages.

For the local meteorological characterization of PW emission sources, 10-m wind speeds and air temperatures were extracted from the Global Data Assimilation System (GDAS: https://www.ncdc.noaa.gov/data...data/...datasets/global-data-assimilation-system-gdas) from Hysplit compatible GDAS meteorological files using MeteoInfo software (Wang, 2014), at 0.5° resolution and at 3-hour intervals, before and after the July 23 of 2014 PW event (i.e., July 22th, 23th, 24th and 25th). Daily composites of synoptic-scale meteorological charts were obtained from the NCEP/NCAR Reanalysis (www.esrl.noaa.gov/psd/data/composites/day/), described in Kalnay et al. (1996).

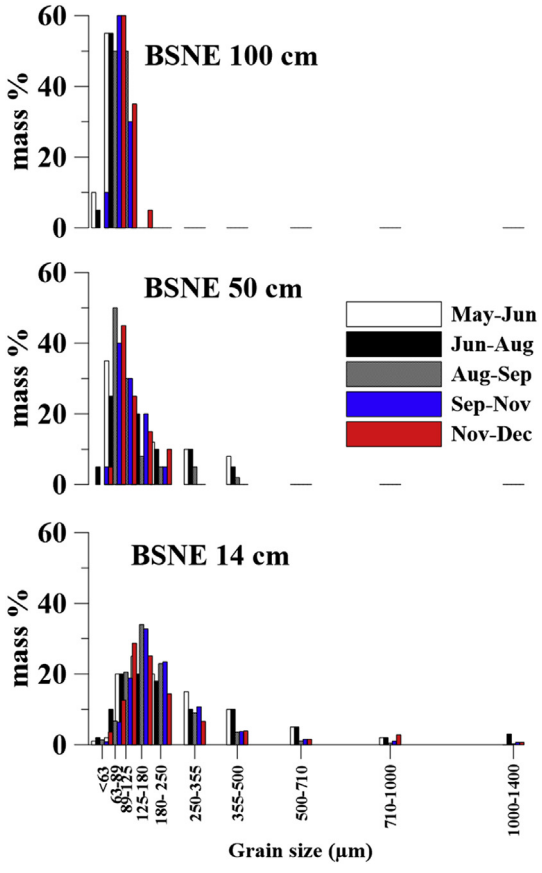

Fig. 2. Grain size (μm) histograms in mass percent for the BSNE samples at 14 cm, 50 cm and 100 cm above ground. Color bars represent sampling time intervals. (For interpretation of the references to colour in this figure legend, the reader is referred to the web version of this article.)

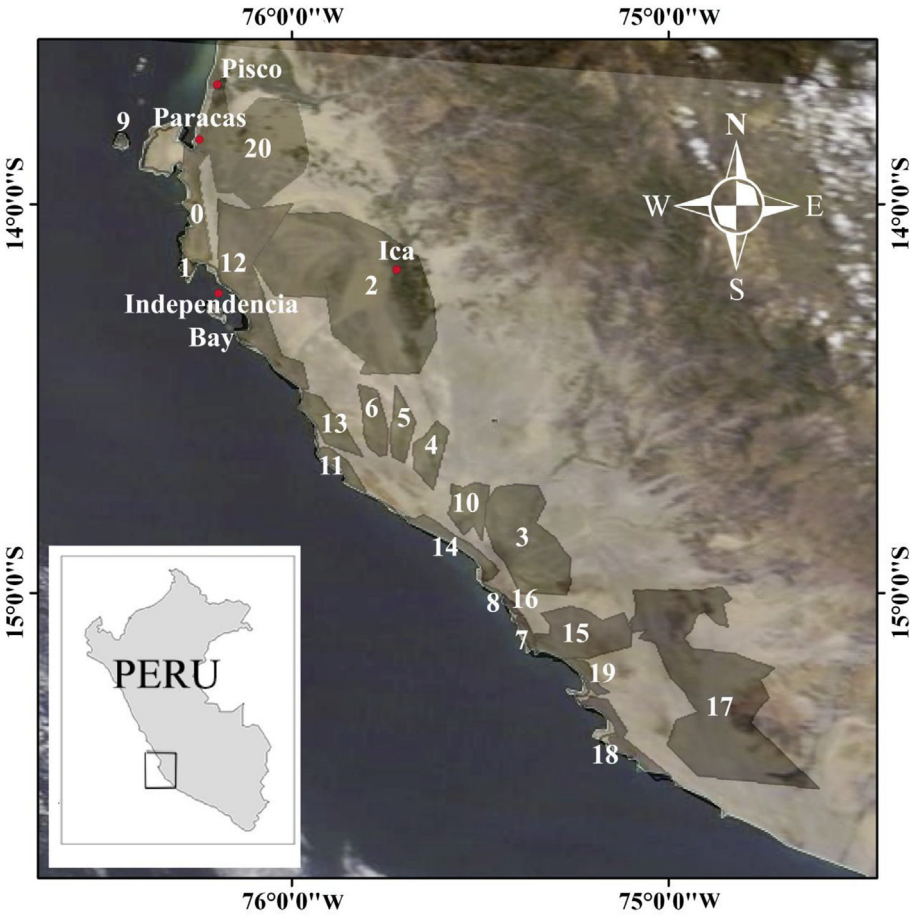

Fig. 3. Dust emission source areas (polygons) identified through visual inspection from Terra and Aqua MODIS imagery.

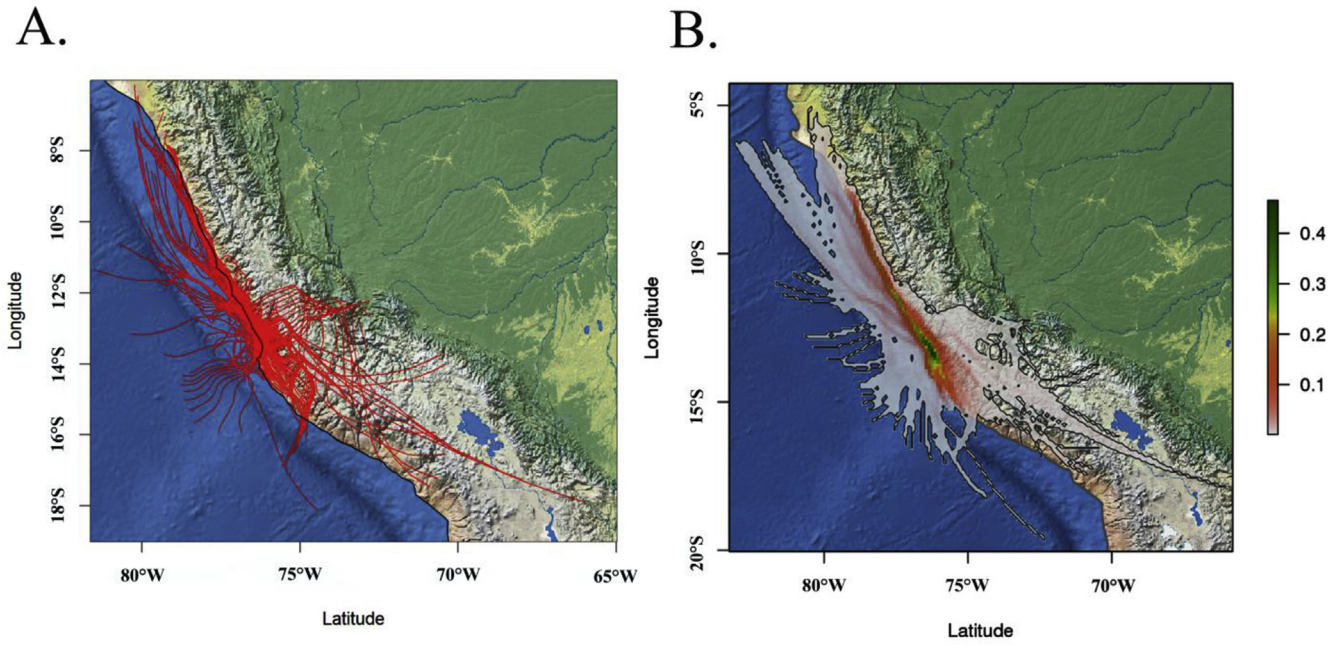

Fig. 4. A) Composite of 845 trajectories for 48 h after each dust emission event. B) Frequency of trajectories considering all dust emission events. The color bar shows the frequency of trajectories that pass through any given grid point. (For interpretation of the references to colour in this figure legend, the reader is referred to the web version of this article.)

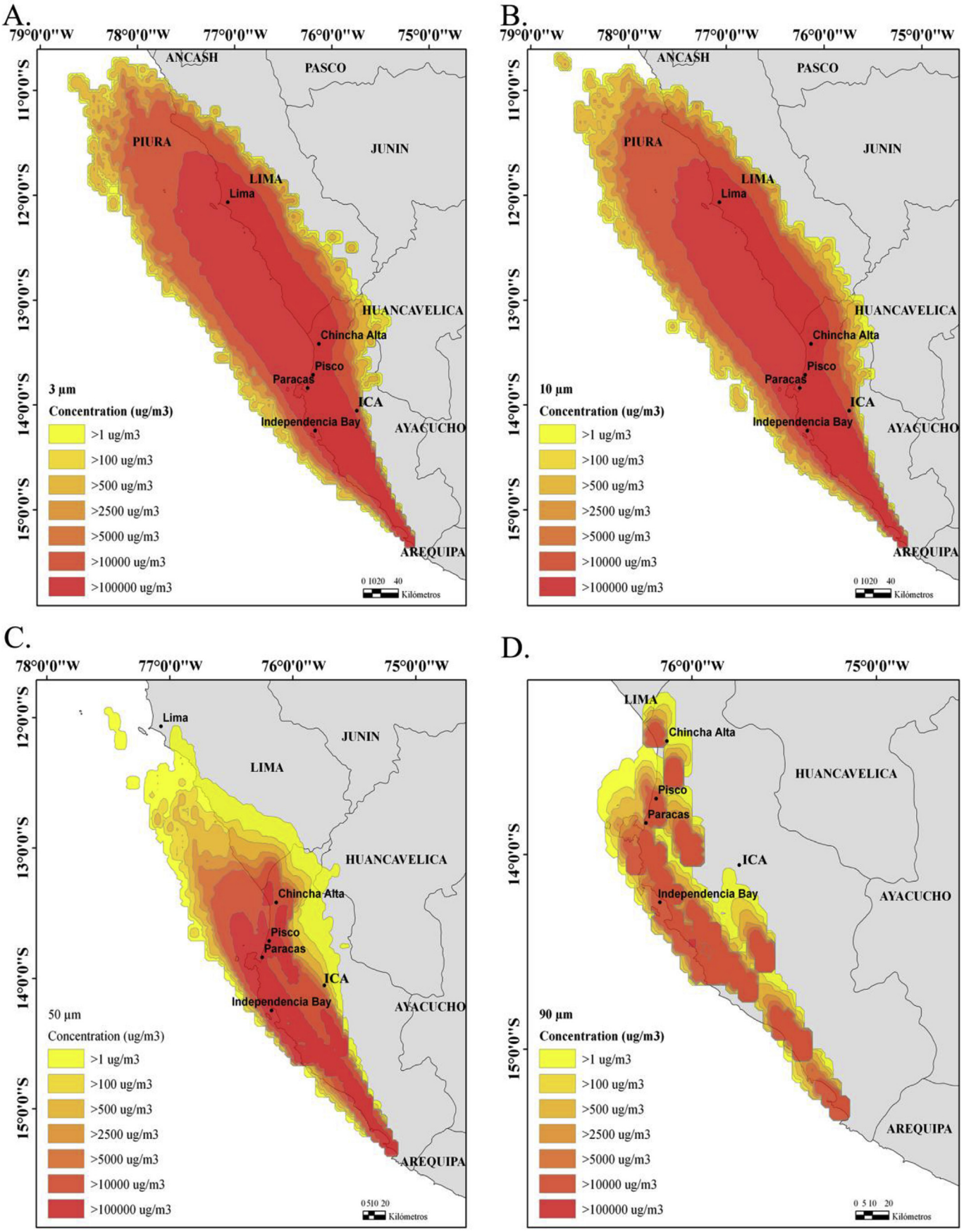

Fig. 5. Particles dispersion and concentration ($\mu g/m^3$) averaged between 0 m and 100 m integrated from 13:00 LT 23 Jul to 13:00 LT 24 Jul, 2014. Release started at 10:00 LT 23 Jul 2014. HYSPLIT model outputs for A) 3 µm, B) 10 µm, C) 50 µm and D) 90 µm particle grain sizes.

Table 1
5-year climatology of (Arica− Pisco) afternoon sea-level pressure (SLP) differences (first line) for the high-sun season semester (HS: October–March) and for the low-sun season one (LS: April–September), together with (SLP-1000) hPa at Arica (second line). At the extremes of the time series, three months instead of six are considered for the HS season: * (January/February/March (JFM), and ** October/November/December (OND). Local time is (UTC-5). 22:00 UTC (17:00 LT) is the time of the maximum wind strength. Standard deviations for the LS season (183 days) are given in parenthesis with bold italics below the corresponding 22:00 UTC means.

UTC	2007		2008		2009		2010		2011		HS[b]
	HS[a]	LS	HS	LS	HS	LS	HS	LS	HS	LS	
17	6	6.9	5.4	5.4	5.2	5.7	5.1	5.9	5.6	6	5.3
	18	24	20	22	20	22	19	23	20	22	21
18	6	6.8	5.5	5.3	5.2	5.7	5	6	5.6	6	5.3
	18	22	20	22	20	21	18	22	20	22	20
19	6.2	7	5.6	5.6	5.6	5.9	5.3	6.3	5.9	6.2	5.8
	18	22	19	21	19	21	18	22	19	21	20
20	6.5	7.4	6	5.9	5.8	6.4	5.5	6.6	6.3	6.5	6
	18	22	19	21	19	20	18	22	19	21	20
21	6.8	7.9	6.5	6.3	6.2	6.7	5.9	7	6.6	7	6.4
	18	22	19	21	19	21	18	22	19	21	20
22	7.3	**8.1**	6.7	**6.7**	6.6	**7**	6.3	**7.3**	7	**7.1**	6.7
		(1.4)		***(1.5)***		***(1.2)***		***(1.6)***		***(1.3)***	
	18	**22**	19	**22**	20	**21**	18	**22**	20	**21**	21
		(2.0)		***(1.8)***		***(2.4)***		***(2.4)***		***(1.9)***	

[a] JFM: January/February/March.
[b] OND: October/November/December.

3. Results and discussion

3.1. Aeolian grain size fractionation

The first size-selective process occurs at the dust emission site. Indeed, it has been widely demonstrated that particles around 100 μm present as loose particles on the soil surface, are the most easy ones to set in motion by saltation under the effect of wind (e.g. Iversen and White, 1982; Kok et al., 2012; Marticorena and Bergametti, 1995; Marticorena, 2014; Shao, 2009). The resulting particle saltation flux displays a finer grain size distribution than its parent soil. A second size-selective process is the vertical entrainment of the particles moving close to the ground level. Due to the natural gravitational size fractionation coarse aeolian material is generally suspended and transported at low altitude, in contrast with the elevated, long-range suspension of the fine-grain material (Iversen and White, 1982; Marticorena, 2014; Shao, 2009).

BSNE Paracas data show that the grain size distribution that can be eroded range from <63 μm to 1400 μm. Besides that, BSNE grain size distributions (Fig. 2) show that, whatever the considered period, samples collected just above the ground level (14 cm height) are dominated by particles with diameters between ~125 and 180 μm, which corresponds to highly erodible soil particles. As the height of the traps increases, the grain size distribution rapidly shifts towards finer particles: particles with diameter between 63 and 125 μm become the most abundant at 50 cm height and are the only ones reaching the highest trap at 100 cm height. This indicates that the 63–125 μm grain size range, is the most easily uplifted and therefore, the most liable to be transported over the Paracas region. These results confirm that these particle range should be used to model a consistent dust emission plume during PW. Additionally, the BSNE results exhibited more particle mass percentage particle capture during austral winter, consistent with previous observations (e.g Quijano, 2013; Escobar, 1993).

3.2. Potential sources of PW erosion events

On the whole we identified 15 emission days (Table 1S) from sharp daily MODIS images (i.e. 2269 used here) in which one or more of the 21 polygonal source-areas were apparent (Fig. 3). A total of 82 dust-plumes (including both Aqua and Terra satellites) yielded 65 independent plumes (one per day per source area) within the selected 15 days. The widespread dust plume variability with regard to specific sources, suggests that emission processes vary within a wide range of extension and intensity. As observed in MODIS images, the coastal region of the Ica desert proved to contribute the most with active emission (Table S1). This erosion-sensitive area features numerous aeolian deposits (Haney and Grolier, 1991), apparently connected with the Northern Ica ones. In addition, satellite images show that most of this material actually drifts northwestward towards the ocean. However, as suggested by Gay (2005), a significant fraction of the blowing material is actually transported into the continent over the Pisco-Paracas area.

3.3. Aeolian trajectory, dispersion and deposition patterns during PW dust storms

The air parcel trajectory modeling for all identified dust emission sources (i.e., 21) resulted in a total of 845 trajectories (Fig. 4A), allowing for the identification of preferred particle pathways for all dust transport events. Assuming that during these events all sources might come to emit material. These results confirm that after emission most of the dust plumes follow alongshore equatorward trajectories, without crossing the Andes during the time domain of the calculations. A kernel composition of these air trajectories shows their spatial frequency of occurrence; suggesting that dust particles are transported both to the nearby ocean as well as inland (Fig. 4B).

The HYSPLIT PW dust emission, concentration and dispersion model results for each grain size mode (i.e., 3 μm, 10 μm, 50 μm and 90 μm) are illustrated in Fig. 5. In particular, 3 μm particle plumes (Fig. 5A) spread northwestward (alongshore) up to 300 km from the emission sources, leading to high dust concentration over some principal Peruvian coastal towns and the adjacent coastal ocean. Besides, the model shows that once the dust has reached the Paracas Peninsula, the plume turns eastward into the continent, highlighting a cyclonic atmospheric circulations, first described in Craig and Psuty (1968). Due to their characteristics, these particles are likely originated during PW by impact of saltating grains or sandblasting (Alfaro et al., 1997; Gomes et al., 1990; Kok et al., 2012; Marticorena, 2014; Shao, 2009) and as long range transport dust (Rea, 1994).

10 μm particles (Fig. 5B) have a dispersion pattern very similar to the 3 μm ones, suggesting that these particles might also remain in suspension for a long time, being therefore also transported over long distances. Results also show that during PW events, particle concentrations can reach above 10^5 μgm^{-3} over the principal coastal towns. According to Naimabadi et al. (2016), Nourmoradi et al. (2015) and Soy et al. (2016) these fine particle concentration could be responsible for increased occurrence of respiratory diseases in populated areas. The origin of these particles might also be sought in the mechanical release by sandblasting. In contrast, the paleoceanographic record of these particles seems to be more complicated since the detrital material from fluvial input has the same grain size distribution and is found in greater proportion than aeolian material (Briceño Zuluaga et al., 2016; Salvatteci et al., 2014).

In contrast, dust plume simulations for 50 μm particles (Fig. 5C) show that they are dispersed downwind reaching up to 80 km from the source, where concentrations exceed 10^4 μgm^{-3}. Results also suggest that these particles are probably generated by saltation and short suspension episodes (Kok et al., 2012; Marticorena, 2014; Shao, 2009). Resulting trajectories (not shown) indicate that this aeolian material is also dispersed both into land, reaching Paracas

Table 2
Dust storm (DS) reported at 22:00 UTC at Pisco (SPSO) between 2007 and 2011 and 2014 during the low-sun season, and associated meteorological conditions: DS strength (number of DS reported hours), wind speed and direction, SLP at SPSO (Pisco) and SCAR (Arica) airfields. SLP means during dust storms for each year can be compared with the corresponding entire seasonal means and standard deviations (in parenthesis) for each year.

Dust Storm						Entire season	
Date	Strength	DD/FF	SLP (hPa)		ΔSLP	SLP_{SCAR}	ΔSLP
	hrs	deg/ms^{-1}	SCAR	SPSO			
2007 Jun 01	3	220/9.25	1024	1012.5	11.5	1022 (2.0)	8.1 (1.4)
2007 Aug 6	5	230/8.74	1026	1016.5	9.5		
2007 Aug 9	3	230/9.25	1026	1014.5	11.5		
2007 Aug 24	4	220/13.37	1024	1016.5	7.5		
2007 Aug 25	4f (5)	220/11.31	1026	1016.5	9.5		
2007 Sep 23	6	230/8.74	1024	1015.5	8.5		
Mean			**1025.0**		**9.7**		
2008 Jul 29	4	220/11.31	1025	1016.5	8.5	1022 (1.8)	6.7 (1.5)
2008 Aug 1	4	230/10.28	1023	1014.5	8.5		
2008 Aug 27	3	230/9.25	1026	1017.5	8.5		
2008 Sep 11	3	230/9.25	1021	1014.5	6.5		
!!2008 Sep 19	i3 (4)	230/8.74	1022	1014.5	7.5		
Mean			**1023.4**		**7.9**		
2009 Aug 5	4	230/8.23	1021	1012.5	8.5	1021 (2.4)	7 (1.2)
2009 Sep 3	i3 (4)	230/9.77	1022	1013.5	8.5		
!!2009 Sep 9	6	220/11.83	1023	1012.5	10.5		
2009 Sep 16		220/11.31	1025	1014.5	10.5		
2009 Sep 17	i5f (7)	230/10.80	1024	1012.5	9.5		
2009 Sep 18		240/9.77	1023	1013.5	9.5		
Mean			**1023.0**		**9.5**		
2010 Apr 22	5	230/11.83	1019	1008.5	10.5	1022 (2.4)	7.3 (1.6)
2010 May 16	6	220/12.34	1023	1013.5	9.5		
2010 May 23	5	240/9.25	1022	1011.5	10.5		
2010 Jun 3	4f (5)	230/10.28	1026	1015.5	10.5		
2010 Jun 26	4	210/10.28	1026	1014.5	11.5		
2010 Jun 27	3	190/8.74	1025	1013.5	11.5		
2010 Sep 3	i3 (4)	230/11.31	1026	1016.5	9.5		
2010 Sep 13	4	240/8.74	1022	1012.5	9.5		
Mean			**1023.6**		**10.4**		
2011 Aug 1	5	230/10.28	1024	1013.5	10.5	1021 (1.9)	7.1 (1.3)
2011 Aug 16	3	220/10.28	1023	1014.5	8.5		
2011 Sep 7	3	230/10.80	1025	1014.5	10.5		
Mean			**1024.0**		**9.8**		
!!2014 July 23	6f (14)	330/5.5*	1026	1012.5	13.5	1021 (1.5)	7.2 (1.4)
!!2014 Sept 05	4	240/9.5	1024	1014.5	9.5		
!!2014 Sept 23	5f (7)	240/11.5	1024.5	1012.5	11.5		
Mean			**1024.8**		**11.5**		

i = event initiated the day before; f = event ended the day after; (*) Wind direction/speed were 240/9.5 for July 22 and 240/8.0 for July 24. **!!** = Events that were displayed in MODIS images.

and Chincha Alta towns, and into the ocean south of Independencia Bay, within the first hour from their emission.

Coarsest 90 μm particles (Fig. 5D) are also likely emitted by saltation processes and transported by suspension, reaching up to 50 km downwind from the sources. McTainsh et al. (1997) and Flores-Aqueveque et al. (2015, 2009) highlight the regional and local character of these particles during the erosive emission processes. Nevertheless, Betzer et al. (1988); Glaccum and Prospero (1980) and Goudie and Middleton (2001) have found that these giant particles can be transported downwind for long ranges. In their experiments Iversen and White (1982); Kok et al. (2012); Marticorena and Bergametti (1995); Marticorena (2014) and Shao (2009) demonstrated that particles between 50 and 110 μm, need a lower threshold surface friction velocity (U*t) (i.e, ~0.20 ms^{-1}).

Model plumes for these coarse particles suggest that, for sources close to the coastline, particles can be directly winnowed into the ocean, being therefore able to reach the Pisco continental shelf. These particles have a short residence time in the water column, so they might be found in a limited number of marine sediment cores of Peruvian coast. These results support the aeolian origin of the coarser lithogenic particles preserved at marine sediment cores from the continental shelf (Briceño Zuluaga et al., 2016). Finally, these results reveal a good match between model dispersion plumes and the MODIS true color image composites.

3.4. Meteorological conditions associated to the PW dust storms

A 5-year climatology of hourly afternoon APGs, calculated as sea-level pressure (SLP) differences between Arica (SCAR) at ~18°28′S and Pisco (SPSO) at ~13°43′S, is presented in Table 1, together with (SLP-1000) hPa at Arica. The largest APGs occur at 17:00 LT (22:00 UTC) in the low-sun season (April–September. Individual dust storm reports (DS) at SPSO for the low-sun seasons of 2007 through 2011 at 17:00 LT (22:00 UTC) are presented in Table 2, with their corresponding strength [number of hours with DS in the METAR reports between 14:00 and 17:00 LT (17:00 and 22:00 UTC)], SPSO wind direction (DD in degrees) and speed (FF in m s^{-1}), SLP (hPa) at SCAR and SPSO, and their difference ΔSLP, as a proxy of the regional APG. For reference, climatological mean values and standard deviations from Table 1 are also included. It can be inferred from Table 2 that ΔSLP during DS stay above 1.14 (2007), 0.8 (2008), 2.1 (2009), 1.9 (2010) and 2.1 (2011) standard deviations from the seasonal average. Associated negative SLP anomalies only at SPSO are 6/28 (21%) while positive ones only at SCAR are 13/28 (46%), the remaining 32% (9/28) correspond to cases in which both negative/positive SLP anomalies appear at SPSO/

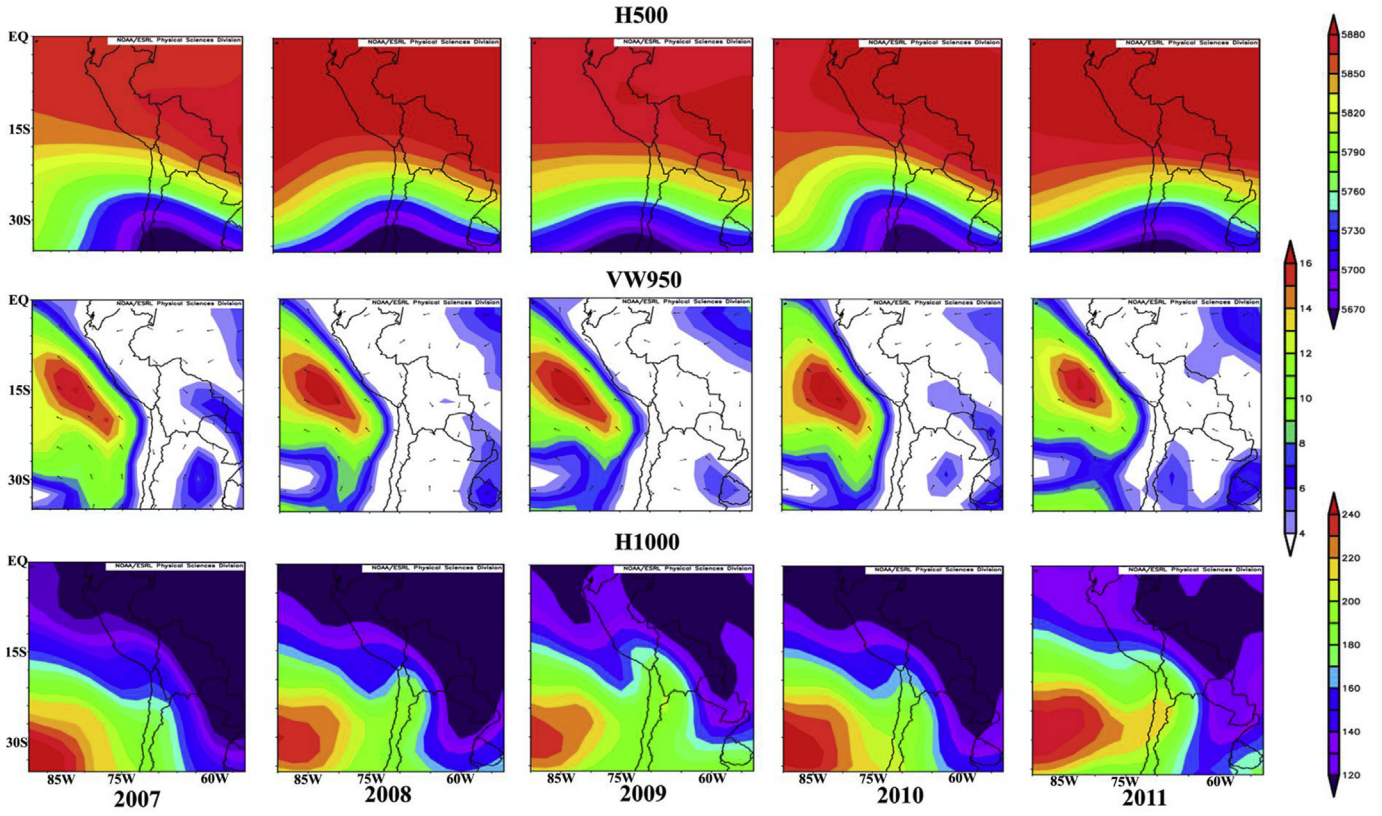

Fig. 6. Synoptic-scale meteorological chart composites for Dust Storms (DS) at Pisco airfield during the low-sun season (April–September) of each year (2007–2011) from the NCEP/NCAR Reanalysis. Top panels represent 500 hPa geopotential heights (H500), middle panels illustrate vector winds at 950 hPa (VW950) and lower panel depict 1000 hPa geopotential heights (H1000).

SCAR, the latter being dominated by the SCARS's positive SLP anomalies that, on the average, stay around one standard deviation above the seasonal mean. Overall, the importance of positive SLP anomalies at SCAR in forcing an enhanced APG along southern Peru calls for a synoptic-scale meteorological control of these PW events, as illustrated in the next paragraph. North of Pisco, Lima and Trujillo reduced SLP data during PW resulted ~1 hPa and ~2 hPa above the SPSO values (not shown), respectively, suggesting a deepening of the coastal thermal trough in the Ica desert, as early described by the cyclonic circulation around the Paracas Peninsula-Pisco Bay area in Schweigger (1968) and Craig and Psuty (1968).

A comparison between PW strength and SLP (METAR) data, considering only five days when MODIS/Aqua observations were available (i.e., 2008/09/19; 2009/09/09; 2014/07/23, 24, 25; 2014/09/05 and 2014/09/23) yields a linear fit explaining 80% of the variance (Fig. 1S), although the scarcity of these simultaneous METAR/MODIS data for clearly observed MODIS dust plumes prevents any significant statistical inference. Besides that, the strength of the PW events also seems directly related to the number of active sources, in particular those nearby Pisco airfield (Table 2S). One source for the lack of simultaneous MODIS/METAR data is the time offset of the Aqua satellite passes (13:30 LT) with respect to the time of the highest wind speeds at SPSO (i.e., 17:00 LT).

Mean wind speeds during DS reported at 17:00 LT (22:00 UTC) at SPSO range from c.a. 8.5–12 m s^{-1} within a direction spanning from 210 to 240° (Southwest winds). Strong alongshore coastal winds (South to Southeast components) shift inlan to SW winds, responsible for the PW dust storms, are also closely related to coastal upwelling. During the last decades these winds have experienced an apparent intensification (e.g., Sydeman et al., 2014). This phenomenon is consistent with the negative trend in sea surface temperature (SST) at Pisco (Gutiérrez et al., 2011), also documented in northern Chile by Falvey and Garreaud (2009), suggesting a wind-driven coastal upwelling intensification. Both, England et al. (2014) and McGregor et al. (2014), while documenting this trend, relate it to the current anthropogenic signal in global climate change. Though an increase in the alongshore wind strength could enhance the intensity or frequency of the PW in a future, as has been reported in the past for northern Chile coast (Flores-Aqueveque et al., 2015), model results reported in Belmadani et al. (2013) predict a slackening of the alongshore winds along the Peruvian coast, in connection with the poleward expansion of the Hadley cell, considered as a robust feature of the regional global warming (e.g., Johanson and Fu, 2009).

3.5. Synoptic weather conditions

Escobar (1993) first documented for a particular PW event the presence of a deep trough in the middle troposphere, with a Northwest/Southeast (NW/SE) oriented axis, that rapidly drifts across the Chilean coast, with maximum wind speeds at about the 950 hPa level. Often these deep troughs segregate a cutoff low, as the eastward-drifting ridge behind the trough overtakes it south of the study area.

Mid troposphere (500 hPa) and near surface (1000 hPa) geopotential heights, together with wind vectors at the 925 hPa level, are composited (Fig. 6), for the PW storms (DS) occurring each low-sun season (April to September) within the 5-year period (Table 2). Although the compositing procedure smooths the resulting patterns due to slight differences in amplitude and position of the

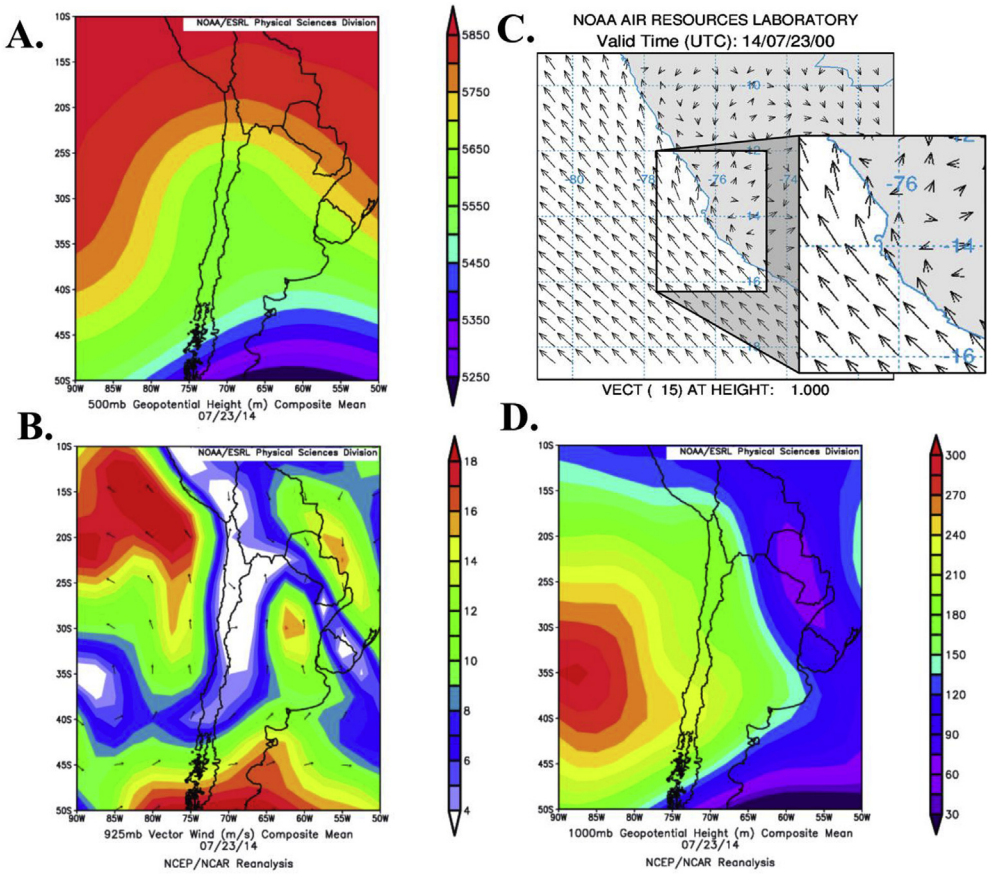

Fig. 7. Synoptic-scale meteorological conditions for the PW event on July 23, 2014: a) Mean 500 hPa geopotential heights from NCEP/NCAR Reanalysis; b) Mean vector winds at 1000 m altitude from GDAS (NOAA ARL), zooming in into the study area; c) Mean vector winds at 925 hPa from NCEP/NCAR Reanalysis; and d) Mean 1000 hPa geopotential heights from NCEP/NCAR Reanalysis.

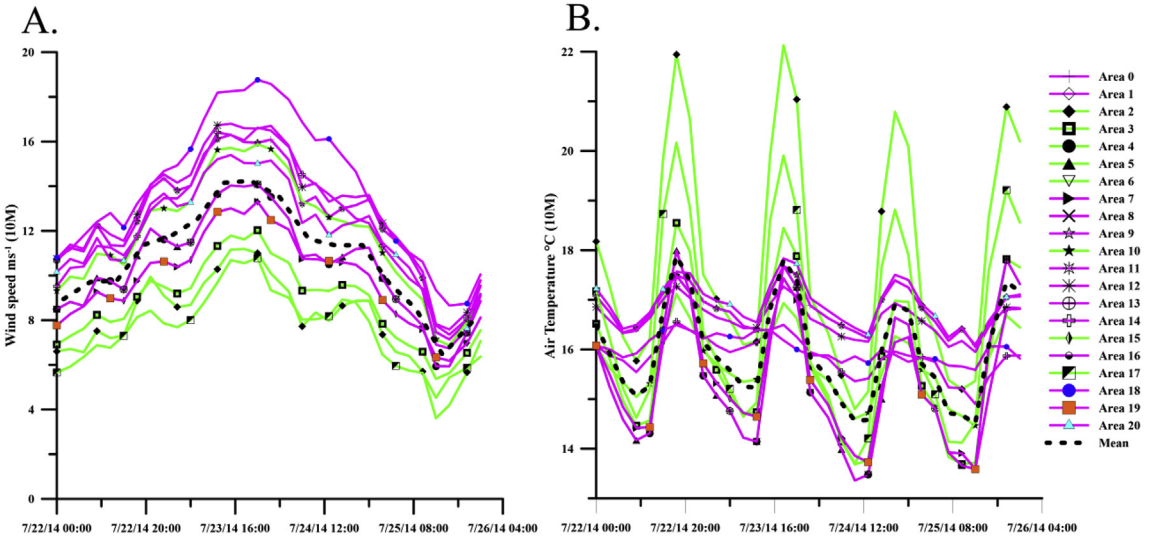

Fig. 8. NOAA ARL 10-m: A) wind speed (ms^{-1}) and B) air temperature (°C), from July 22 (00:00 LT) to July 25 (21:00 LT) 2014 at 3 h intervals (GDAS 0.5°) at the center of all identified emission-source areas. Purple and green lines indicate coastal and inland source areas, respectively. The dashed black lines represent averages over all emission sources. (For interpretation of the references to colour in this figure legend, the reader is referred to the web version of this article.)

main synoptic-scale features, the 500 hPa composites show the trough location over central Chile whereas the 1000 hPa composites suggest a strengthening of the anticyclonic conditions in northern Chile (i.e. SCAR positive SLP anomalies) that can be attributed to the cold air advection associated with the deep trough in the middle troposphere. Stronger southerlies along southern Peru would then be due to a reinforced subtropical anticyclone fostered by cold air advection in connection with the elongated,

deep through along northern Chile. A thorough discussion of the attending meteorological conditions before, during and after strong winds in southern Peru as seen in the CFSR reanalysis, is given in Rahn and Garreaud (2013) who include surface convergence at the coastline bend along the Peru-Chile border (17–18°S) to partially explain the positive SLP anomaly at Arica.

Mean meteorological charts for July 23th, 2014, for which the HYSPLIT dust trajectories were simulated, are given in Fig. 7. A deep ridge-trough wave pattern with the trough axis just over central Chile is already apparent, consistent with the composites depicted in Fig. 6 and with Escobar (1993) weather map. GDAS mean surface air temperatures show a general increase exceeding 2 °C in the preceding afternoon and in the morning of the PW. In addition, a difference of ~4 °C is evident between the coastal and inland emission points, showing a strong temperature gradient, particularly during the afternoon (Fig. 8). Wind velocity reached a mean of ~15 ms^{-1} at 17:00 LT on the same PW day (Fig. 8). These velocities, in combination with the surface geomorphological data, are consistent with a required threshold surface friction velocity of ~0.20 ms^{-1} for the dust-emission onset of dust particles spanning the 60–100 μm range (present on the Paracas soils), as documented in Iversen and White (1982); Kok et al. (2012); Marticorena (2014) and Shao (2004). Quijano (2013) using a regional numerical simulation model (MM5) and complementary fieldwork with BSNE traps on the Paracas peninsula, observed a local threshold surface friction velocity of 0.72 ms^{-1}. This value largely exceeds those proposed by Iversen and White (1982); Kok et al. (2012); Marticorena (2014) and Shao (2004) for grain size modes captured by the BSNE traps. A discussion on the disagreement I thlocal threshold surface friction velocity is beyond the scope of the present work, requiring probably further extensive field work and numerical simulations. However Quijano (2013), experiments highlighted the importance of solar radiation and coast-inland thermal gradient as relevant for the onset of PW, also confirming a northwestward aeolian transport towards the Paracas, Pisco and Chincha towns. Our results suggest that probably most of the dust sources have a lower threshold surface friction velocity, coherent in our simulation with MODIS particle dispersion patterns.

4. Conclusions

Results from the HYSPLIT emission and dispersion model complemented with visual inspection of MODIS satellite imagery have proved to be efficient tools in a synoptic assessment of the development and evolution of PW events. Compared to the MODIS images, HYSPLIT was able to spatially reproduce the trajectory and plume dispersion during PW. Results show that particles moving into the Ica region are emitted at the coastal zone, where winds are stronger during PW events. HYSPLIT simulation show that the saltation and suspension mechanisms are probably the most important for the displacement of the coarser particles during PW. These strong winds are forced by anomalously strong alongshore pressure gradients in which rising SLP south of the study area (Arica) dominates over falling SLP at Pisco. Synoptic-scale meteorological composites from NCEP/NCAR reanalysis data show that PW events are associated with the strengthening of the anticyclonic conditions in northern Chile, that can be attributed to cold air advection associated with a deep trough in the middle troposphere over north-central Chile. The case study of the PW event on July 23, 2014 confirms these results. Direct relationships between Paracas wind intensity, number of active dust-emission sources in MODIS imagery and APGs are also documented, although the scarcity of simultaneous METAR/MODIS data for clearly observed MODIS dust plumes prevents any significant statistical inference. The presence of the aeolian signal in the continental shelf sediments is assessed, being thus of great importance for paleo-environmental studies. The results also show that the population in Pisco and Chincha Alta towns can be affected by high particle concentrations during PW.

Acknowledgements

This work was supported by the International Joint Laboratory "PALEOTRACES" (IRD-France, UPMC-France, UFF-Brazil, UA-Chile, UPCH-Peru), the Department of Geochemistry of the Universidade Federal Fluminense-UFF (Brazil), the Peruvian Marine Research Institute (IMARPE) and the Geophysical Peruvian Institute (IGP). It was also supported by the collaborative project Chaire Croisée PROSUR (IRD). The authors gratefully acknowledge the NOAA Air Resources Laboratory (ARL) for the provision of the HYSPLIT transport and dispersion model and READY website (http://www.arl.noaa.gov/ready.php) used in this publication. We also acknowledge the use of Rapid Response imagery from the Land, Atmosphere Near real-time Capability for EOS (LANCE) system operated by the NASA/GSFC/Earth Science Data and Information System (ESDIS) with funding provided by NASA/HQ. We deeply thank the CAPES-Brazil and FAPERJ (2014.00479.0) for the scholarship to Francisco Briceño Zuluaga. V. Flores-Aqueveque acknowledges funding from FONDECYT-Chile projects 11121543 and NC120066. We are also grateful to the anonymous reviewers for their constructive and helpful suggestions to improve this manuscript.

Appendix A. Supplementary data

Supplementary data related to this article can be found at http://dx.doi.org/10.1016/j.atmosenv.2017.06.019.

References

Achudume, A.C., Oladipo, B.O., 2009. Effects of dust storm on health in the nigerian environment. Biol. Med. 1, 21–27.

Alfaro, S.C., Gaudichet, A., Gomes, L., Maillé, M., 1997. Modeling the size distribution of a soil aerosol produced by sandblasting. J. Geophys. Res. Atmos. 102 (D10), 11239–11249.

Belmadani, A., Echevin, V., Codron, F., Takahashi, K., Junquas, C., 2013. What dynamics drive future wind scenarios for coastal upwelling off Peru and Chile? Clim. Dyn. 43, 1893–1914. http://dx.doi.org/10.1007/s00382-013-2015-2.

Betzer, P.R., Carder, K.L., Duce, R.A., Merrill, J.T., Tindale, N.W., Uematsu, M., Costello, D.K., Young, R.W., Feely, R.A., Breland, J.A., Bernstein, R.E., Greco, A.M., 1988. Long-range transport of giant mineral aerosol particles. Nature 336, 568–571. http://dx.doi.org/10.1038/332141a0.

Briceño Zuluaga, F., Sifeddine, A., Caquineau, S., Cardich, J., Salvatteci, R., Gutierrez, D., Ortlieb, L., Velazco, F., Boucher, H., Machado, C., 2016. Terrigenous material supply to the Peruvian central continental shelf (Pisco 14° S) during the last 1000 yr: paleoclimatic implications. Clim. Past. 12, 787–798. http://dx.doi.org/10.5194/cpd-12-787-2016.

Craig, A. k, Psuty, N.P., 1968. The Paracas papers. Stud. Mar. Desert Ecol. 1, 198.

Dewitte, B., Illig, S., Renault, L., Goubanova, K., Takahashi, K., Gushchina, D., Mosquera, K., Purca, S., 2011. Modes of covariability between sea surface temperature and wind stress intraseasonal anomalies along the coast of Peru from satellite observations (2000-2008). J. Geophys. Res. Ocean. 116, 1–16. http://dx.doi.org/10.1029/2010JC006495.

Draxler, R.R., Gillette, D.A., Kirkpatrick, J.S., Heller, J., 2001. Estimating PM10 air concentrations from dust storms in Iraq, Kuwait and Saudi Arabia. Atmos. Environ. 35, 4315–4330. http://dx.doi.org/10.1016/S1352-2310(01)00159-5.

Draxler, R.R., Hess, G.D., 1998. An overview of the HYSPLIT_4 modelling system for trajectories, dispersion, and deposition. Aust. Meteorol. Mag. 47, 295–308.

England, M.H., McGregor, S., Spence, P., Meehl, G. a., Timmermann, A., Cai, W., Gupta, A. Sen, McPhaden, M.J., Purich, A., Santoso, A., 2014. Recent intensification of wind-driven circulation in the Pacific and the ongoing warming hiatus. Nat. Clim. Chang. 4, 222–227. http://dx.doi.org/10.1038/nclimate2106.

Escobar, D.F., 1993. Evaluación climatológica y sinóptica del fenómeno de vientos Paracas. Lima, Perú. Tesis para optar el titulo de Ingeniero Meteorologico. Universidad Nacional Agraria La Molina, 62pp.

Escudero, M., Stein, A., Draxler, R.R., Querol, X., Alastuey, A., Castillo, S., Avila, A., 2006. Determination of the contribution of northern Africa dust source areas to PM10 concentrations over the central Iberian Peninsula using the Hybrid Single-Particle Lagrangian Integrated Trajectory model (HYSPLIT) model. J. Geophys. Res. Atmos. 111, 1–15. http://dx.doi.org/10.1029/2005JD006395.

Falvey, M., Garreaud, R.D., 2009. Regional cooling in a warming world: recent temperature trends in the southeast Pacific and along the west coast of subtropical South America (1979-2006). J. Geophys. Res. Atmos. 114, 1–16. http://dx.doi.org/10.1029/2008JD010519.

Flores-Aqueveque, V., Alfaro, S., Vargas, G., Rutllant, J. a., Caquineau, S., 2015. Aeolian particles in marine cores as a tool for quantitative high-resolution reconstruction of upwelling favorable winds along coastal Atacama Desert. North. Chile. Prog. Oceanogr. 134, 244–255. http://dx.doi.org/10.1016/j.pocean.2015.02.003.

Flores-Aqueveque, V., Vargas, G., Rutllant, J., Le Roux, J.P., 2009. Estacionalidad de la erosión y el transporte eólico de partículas en el desierto costero de Atacama, Chile (23°S). Andean Geol. 36, 288–310. http://dx.doi.org/10.4067/S0718-71062009000200006.

Fryrear, D., 1986. A field dust sampler. J. Soil Water Conserv. 41, 117–120.

Garreaud, R., Muñoz, R.C., 2005. The low-level jet off the West coast of subtropical south America: structure and variability. Mon. Weather Rev. 133, 2246–2261. http://dx.doi.org/10.1175/MWR2972.1.

Gay, S.P., 2005. Blowing sand and surface winds in the Pisco to Chala area, southern Peru. J. Arid. Environ. 61, 101–117. http://dx.doi.org/10.1016/j.jaridenv.2004.07.012.

Glaccum, R.A., Prospero, J.M., 1980. Saharan aerosols over the tropical North Atlantic — mineralogy. Mar. Geol. 37, 295–321. http://dx.doi.org/10.1016/0025-3227(80)90107-3.

Gomes, L., Bergametti, G., Dulac, F., Ezat, U., 1990. Assessing the actual size distribution of atmospheric aerosols collected with a cascade impactor. J. Aerosol Sci. 21, 47–59. http://dx.doi.org/10.1016/0021-8502(90)90022-P.

Goudie, A.S., Middleton, N.J., 2001. Saharan dust storms: nature and consequences. Earth-Science Rev. 56, 179–204. http://dx.doi.org/10.1016/S0012-8252(01)00067-8.

Gutiérrez, D., Bouloubassi, I., Sifeddine, A., Purca, S., Goubanova, K., Graco, M., Field, D., Méjanelle, L., Velazco, F., Lorre, A., Salvatteci, R., Quispe, D., Vargas, G., Dewitte, B., Ortlieb, L., 2011. Coastal cooling and increased productivity in the main upwelling zone off Peru since the mid-twentieth century. Geophys. Res. Lett. 38, 1–6. http://dx.doi.org/10.1029/2010GL046324.

Haney, E.M., Grolier, M.J., 1991. Geologic Map of Major Quaternary Eolian Features, Northern and Central Coastal Peru, United States Geological Survey, Miscellaneous Investigations Report. USGS Numbered Series. https://pubs.er.usgs.gov/publication/i2162.

Ingram, R., 1971. Sieve analysis. In: Procedures in Sedimentary Petrology. John Wiley & Sons, Inc., pp. 49–67

Iversen, J.D., White, B.R., 1982. Saltation threshold on earth, mars and Venus. Sedimentology 29, 111–119. http://dx.doi.org/10.1111/j.1365-3091.1982.tb01713.x.

Johanson, C.M., Fu, Q., 2009. Hadley cell widening: model simulations versus observations. J. Clim. 22, 2713–2725. http://dx.doi.org/10.1175/2008JCLI2620.1.

Kalnay, E., Kanamitsu, M., Kistler, R., Collins, W., Deaven, D., Gandin, L., Iredell, M., Saha, S., White, G., Woollen, J., Zhu, Y., Leetmaa, A., Reynolds, R., Chelliah, M., Ebisuzaki, W., Higgins, W., Janowiak, J., Mo, K.C., Ropelewski, C., Wang, J., Jenne, R., Joseph, D., 1996. The NCEP/NCAR 40 Year reanalysis project. Bull. Am. Meteorol. Soc. 77, 437–471.

Kok, J.F., Parteli, E.J.R., Michaels, T.I., Karam, D.B., 2012. The physics of wind-blown sand and dust. Rep. Prog. Phys. 75, 106901. http://dx.doi.org/10.1088/0034-4885/75/10/106901.

Marticorena, B., 2014. Dust production mechanisms. In: Knippertz, P., Stuut, J.-B. (Eds.), Mineral Dust: a Key Player in the Earth System. Springer, New York, pp. 93–120. http://dx.doi.org/10.1007/978-94-017-8978-3.

Marticorena, B., Bergametti, G., 1995. Modeling the atmospheric dust cycle .1. Design of a soil-derived dust emission scheme. J. Geophys. Res. http://dx.doi.org/10.1029/95jd00690.

McGregor, S., Timmermann, A., Stuecker, M.F., England, M.H., Merrifield, M., Jin, F.-F., Chikamoto, Y., 2014. Recent Walker circulation strengthening and Pacific cooling amplified by Atlantic warming. Nat. Clim. Chang. 4, 888–892. http://dx.doi.org/10.1038/nclimate2330.

McTainsh, G.H., Nickling, W.G., Lynch, a. W., 1997. Dust deposition and particle size in Mali, West Africa. Catena 29, 307–322. http://dx.doi.org/10.1016/S0341-8162(96)00075-6.

Muñoz, R.C., Garreaud, R., 2005. Dynamics of the low-level jet off the West coast of subtropical south America. Mon. Weather Rev. 133, 3661–3677. http://dx.doi.org/10.1175/MWR3074.1.

Naimabadi, A., Ghadiri, A., Idani, E., Babaei, A.A., Alavi, N., Shirmardi, M., Khodadadi, A., Marzouni, M.B., Ankali, K.A., Rouhizadeh, A., Goudarzi, G., 2016. Chemical composition of PM10 and its in vitro toxicological impacts on lung cells during the Middle Eastern Dust (MED) storms in Ahvaz. Iran. Environ. Pollut. 211, 316–324. http://dx.doi.org/10.1016/j.envpol.2016.01.006.

Nourmoradi, H., Moradnejadi, K., Moghadam, F.M., Khosravi, B., Hemati, L., Khoshniyat, R., Kazembeigi, F., 2015. The effect of dust storm on the microbial quality of ambient air in sanandaj: a city located in the West of Iran. Glob. J. Health Sci. 7, 46888. http://dx.doi.org/10.5539/gjhs.v7n7p114.

QGIS Development Team, 2016. QGIS Geographic Information System. Open Source geospatial foundation Project. http://www.qgis.org/.

Quijano, J.J., 2013. Estudio numerico y observacional de la dinámica de Viento Paracas, asociado al transporte eólico hacia el océano frente a la costa de Ica-Perú. Universidad Peruana Cayetano Heredia, Lima - Perú. MSc Thesis, 151pp. http://www.met.igp.gob.pe/publicaciones/2013/JQuijano_tesisMSc.pdf.

Rahn, D.A., Garreaud, R.D., 2013. A synoptic climatology of the near-surface wind along the west coast of South America. Int. J. Climatol. 34, 780–792. http://dx.doi.org/10.1002/joc.3724.

Rea, D.K., 1994. The paleoclimatic deposition record provided of wind by eolian in the deep sea: the geolgic history of wind. Rev. Geophys. 32, 159–195.

Rolph, G.D., 2016. Real-time Environmental Applications and Display System (READY). NOAA Air Resour. Lab, Silver Spring, MD [WWW Document]. https://www.ready.noaa.gov/.

Saha, S., Moorthi, S., Pan, H.L., Wu, X., Wang, J., Nadiga, S., Tripp, P., Kistler, R., Woollen, J., Behringer, D., Liu, H., Stokes, D., Grumbine, R., Gayno, G., Wang, J., Hou, Y.T., Chuang, H.Y., Juang, H.M.H., Sela, J., Iredell, M., Treadon, R., Kleist, D., Van Delst, P., Keyser, D., Derber, J., Ek, M., Meng, J., Wei, H., Yang, R., Lord, S., Van Den Dool, H., Kumar, A., Wang, W., Long, C., Chelliah, M., Xue, Y., Huang, B., Schemm, J.K., Ebisuzaki, W., Lin, R., Xie, P., Chen, M., Zhou, S., Higgins, W., Zou, C.Z., Liu, Q., Chen, Y., Han, Y., Cucurull, L., Reynolds, R.W., Rutledge, G., Goldberg, M., 2010. The NCEP climate forecast system reanalysis. Bull. Am. Meteorol. Soc. 91, 1015–1057. http://dx.doi.org/10.1175/2010BAMS3001.1.

Salvatteci, R., Gutierrez, D., Field, D., Sifeddine, A., Ortlieb, L., Bouloubassi, I., Boussafir, M., Boucher, H., Cetin, F., 2014. The response of the Peruvian Upwelling Ecosystem to centennial-scale global change during the last two millennia. Clim. Past. 10, 1–17. http://dx.doi.org/10.5194/cp-10-1-2014.

Schweigger, E., 1968. El Litoral Peruano (Segunda Edición). Universidad Nacional "Federico Villarreal", Lima, Perú, Lima, 435pp.

Shao, Y., 2009. Physics and Modelling of Wind Erosion - Front Matter. In: Mysak, L., Hamilton, K. (Eds.), Physics and Modelling of Wind Erosion. Springer, Germany. http://dx.doi.org/10.1007/978-1-4020-8895-7 i–xv.

Shao, Y., 2004. Simplification of a dust emission scheme and comparison with data. J. Geophys. Res. D. Atmos. 109, 1–6. http://dx.doi.org/10.1029/2003JD004372.

Shao, Y., Wyrwoll, K.-H., Chappell, A., Huang, J., Lin, Z., McTainsh, G.H., Mikami, M., Tanaka, T.Y., Wang, X., Yoon, S., 2011. Dust cycle: an emerging core theme in Earth system science. Aeolian Res. 2, 181–204. http://dx.doi.org/10.1016/j.aeolia.2011.02.001.

Sifeddine, A., Gutiérrez, D., Ortlieb, L., Boucher, H., Velazco, F., Field, D., Vargas, G., Boussafir, M., Salvatteci, R., Ferreira, V., García, M., Valdés, J., Caquineau, S., Mandeng Yogo, M., Cetin, F., Solis, J., Soler, P., Baumgartner, T., 2008. Laminated sediments from the central Peruvian continental slope: a 500 year record of upwelling system productivity, terrestrial runoff and redox conditions. Prog. Oceanogr. 79, 190–197. http://dx.doi.org/10.1016/j.pocean.2008.10.024.

Soy, F.K., Kulduk, E., Do, S., Can, H., 2016. The effects of dust storms on quality of life of allergic patients with or without asthma. Kulak Burun Bogaz Ihtis. Derg. 26, 19–27. http://dx.doi.org/10.5606/kbbihtisas.2016.56254.

Stein, A.F., Draxler, R.R., Rolph, G.D., Stunder, B.J.B., Cohen, M.D., Ngan, F., 2015. Noaa's hysplit atmospheric transport and dispersion modeling system. Bull. Am. Meteorol. Soc. 96, 2059–2077. http://dx.doi.org/10.1175/BAMS-D-14-00110.1.

Suess, E., Kulm, L.D., Killingley, J.S., 1987. Coastal upwelling and a history of organic-rich mudstone deposition off Peru. Geol. Soc. Lond. Spec. Publ. 26, 181–197. http://dx.doi.org/10.1144/GSL.SP.1987.026.01.11.

Sydeman, W.J., García-Reyes, M., Schoeman, D.S., Rykaczewski, R.R., Thompson, S. a, Black, B. a, Bograd, S.J., 2014. Climate change and wind intensification in coastal upwelling ecosystems. Sci. N. Y. 345, 77–80. http://dx.doi.org/10.1126/science.1251635.

Takahashi, K., Gutiérrez, D., Quijano, J., Velazco, F., Gómez, J.C., Quispe, N., Rutllant, J., Siffedine, A., Caquineau, S., Dewitte, B., Montecinos, A., 2011. Dinámica de los vientos, Paracas y transporte eólico de sedimentos al océano. Instituto Geofísico del Perú.

Wang, Y., Stein, A.F., Draxler, R.R., de la Rosa, J.D., Zhang, X., 2011. Global sand and dust storms in 2008: observation and HYSPLIT model verification. Atmos. Environ. 45, 6368–6381. http://dx.doi.org/10.1016/j.atmosenv.2011.08.035.

Wang, Y.Q., 2014. MeteoInfo: GIS software for meteorological data visualization and analysis. Meteorol. Appl. 21, 360–368. http://dx.doi.org/10.1002/met.1345.

Wentworth, C.K., 1922. A scale of grade and class terms for clastic sediments. J. Geol. 30, 377–392. http://dx.doi.org/10.1086/622910.

Westphal, D.L., Toon, O.B., Carlson, T.N., 1987. A two-dimensional numerical investigation of the dynamics and microphysics of Saharan dust storms. J. Geophys. Res. 92, 3027–3049.